JOC Article

$^{13}C-^{13}C$ NMR Spin−Spin Coupling Constants in Saccharides: Structural Correlations Involving All Carbons in Aldohexopyranosyl Rings

Bidisha Bose-Basu,[†] Thomas Klepach,[†] Gail Bondo,[‡] Paul B. Bondo,[‡] Wenhui Zhang,[†] Ian Carmichael,[§] and Anthony S. Serianni*,[†]

Department of Chemistry and Biochemistry and Radiation Laboratory, University of Notre Dame, Notre Dame, Indiana 46556, and Omicron Biochemicals, Inc., 115 South Hill Street, South Bend, Indiana 46617

serianni.1@nd.edu

Received April 2, 2007

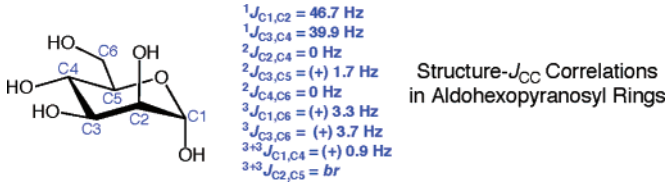

$^{13}C-^{13}C$ Spin−spin coupling constants (J_{CC}) have been measured in a group of aldohexopyranoses and methyl aldopyranosides singly labeled with ^{13}C at different sites to confirm and extend prior correlations between J_{CC} magnitude and sign and saccharide structure. Structural correlations for $^2J_{C1,C3}$, $^2J_{C2,C4}$, $^2J_{C4,C6}$, and $^2J_{C1,C5}$ have been confirmed using density functional theory calculations to test empirical predictions. These geminal couplings depend highly on the orientation of C−O bonds appended to the terminal coupled carbons, but new evidence suggests that $^2J_{CCC}$ values are also affected by intervening carbon structure and C−O bond rotation. $^3J_{C1,C6}$ and $^3J_{C3,C6}$ values show Karplus-like dependences but also are affected by in-plane terminal hydroxyl substituents. In both cases, rotation about the C5−C6 bond modulates the coupling due to the alternating in-plane and out-of-plane O6. $^3J_{C3,C6}$ is also affected by C4 configuration. Both $^3J_{C1,C6}$ and $^3J_{C3,C6}$ are subject to remote effects involving the structure at C3 and C1, respectively. New structural correlations have been determined for $^2J_{C3,C5}$, which, like $^3J_{C3,C6}$, shows a remote dependence on anomeric configuration. Investigations of dual pathway $^{13}C-^{13}C$ couplings, $^{3+3}J_{C1,C4}$ and $^{3+3}J_{C2,C5}$, revealed an important additional internal electronegative substituent effect on $^3J_{CC}$ in saccharides, a structural factor undocumented previously and one of importance to the interpretation of trans-glycoside $^3J_{COCC}$ in oligosaccharides.

Introduction

With increasing applications of ^{13}C-labeled saccharides in studies of their molecular structures and dynamics, $^{13}C-^1H$ and $^{13}C-^{13}C$ spin−spin coupling constants (*J*-couplings; J_{CH}, J_{CC}) are expected to increase in importance as tools to confirm and/or extend structural conclusions based on $^1H-^1H$ spin-couplings, nuclear spin relaxation, $^1H-^1H$ NOE, and other data. In contrast to some of the latter NMR parameters, however, present understanding of J_{CH} and J_{CC} in saccharides is incomplete, thereby limiting more routine use. This deficiency is more pronounced for J_{CC} than for J_{CH} primarily because measurement of the former generally requires isotopic labeling, while the latter can be obtained on samples at natural abundance, although often less conveniently and with reduced accuracy.[1]

J_{CC} values in carbohydrates across one ($^1J_{CC}$), two ($^2J_{CCC}$, $^2J_{COC}$), and three ($^3J_{CCCC}$, $^3J_{COCC}$) bonds (Scheme 1) have been reported in aldohexopyranoses singly ^{13}C-labeled at the anomeric[2] (C1) and hydroxymethyl[3] (C6) carbons. These studies

* Corresponding author. Tel.: (574) 631-7807; fax: (574) 631-6652.
† Department of Chemistry and Biochemistry, University of Notre Dame.
‡ Omicron Biochemicals, Inc.
§ Radiation Laboratory, University of Notre Dame.

(1) (a) Blechta, V.; del Rio-Portilla, F.; Freeman, R. *Magn. Reson. Chem.* **1994**, *32*, 134−137. (b) Nishida, T.; Widmalm, G.; Sandor, P. *Magn. Reson. Chem.* **1995**, *33*, 596−599.
(2) King-Morris, M. J.; Serianni, A. S. *J. Am. Chem. Soc.* **1987**, *109*, 3501−3508.
(3) Wu, J.; Bondo, P. B.; Vuorinen, T.; Serianni, A. S. *J. Am. Chem. Soc.* **1992**, *114*, 3499−3505.

10.1021/jo0706776 CCC: $37.00
Published on Web 09/07/2007

SCHEME 1. Representative $^{1}J_{CC}$, $^{2}J_{CC}$, $^{3}J_{CC}$, and $^{3+3}J_{CC}$ in Methyl β-D-Glucopyranoside[a]

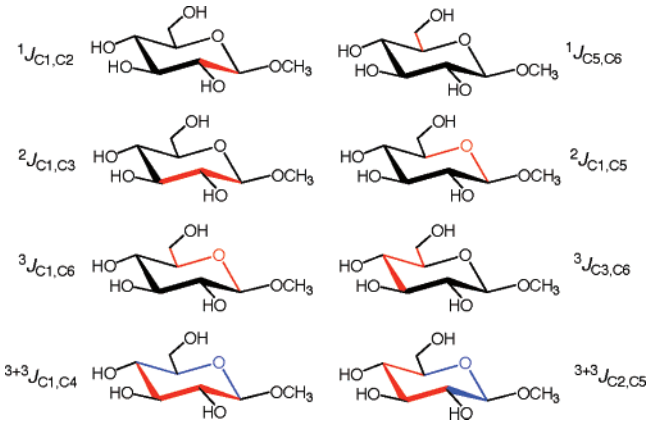

[a] Coupling pathways are in red and blue.

have provided a limited data set with which to develop generalized structure/*J*-coupling correlations. Bossennec *et al.*[4] have reported complete sets of J_{CC} values in α-D-glucopyranose, β-D-glucopyranose, 1,2;5,6-di-*O*-isopropylidene-α-D-glucofuranose, and 1,2;5,6-di-*O*-isopropylidene-3-*O*-benzyl-α-D-glucofuranose using uniformly ^{13}C-labeled compounds, and Krivdin and Kalabin[5] have reported some general correlations between $^{1}J_{CC}$ and carbohydrate structure. Church *et al.*[6] have proposed an empirical (projection resultant; PR) method to predict $^{2}J_{CCC}$ and $^{2}J_{COC}$, Bose *et al.*[7] and Cloran *et al.*[8] have derived Karplus relationships for $^{3}J_{COCC}$, and experimental sign determinations for $^{2}J_{CCC}$ and $^{2}J_{COC}$ have been reported.[9,10] A C−O−C bond angle dependence has been described for $^{2}J_{COC}$ in saccharides.[11] These previous studies have demonstrated the potential of J_{CC} values as structural and conformational probes, especially in conformationally flexible systems (e.g., α-idopyranosyl and aldofuranosyl rings and *O*-glycosidic linkages). However, given the relatively limited scope of prior work (e.g., J_{CC} studies confined mainly to C1 and C6 of aldohexopyranosyl rings), further investigations of J_{CC} involving C2−C5 of aldopyranosyl rings are essential to assess the general applicability of prior structural relationships and to promote the potential discovery of new relationships.

In this paper, studies of ^{13}C−^{13}C spin-coupling constants in monosaccharides have been extended significantly to include a broad range of aldohexopyranosyl rings selectively labeled with ^{13}C at sites other than C1 and C6, thereby allowing accurate determinations of J_{CC} involving C2−C5 as a function of ring configuration and conformation. Prior correlations between J_{CC} and molecular structure involving C1 and C6 have been confirmed, extended, and/or modified, and new structural relationships for several single and dual pathway J_{CC}, specifically, $^{2}J_{C3,C5}$, $^{3+3}J_{C1,C4}$, and $^{3+3}J_{C2,C5}$, are proposed. Structural correlations derived from the interpretation of previously reported, and newly measured, J_{CC} values have been validated and refined through theoretical calculations of J_{CC} using density functional theory (DFT). The findings reported herein contribute to the long-range goal of providing complete interpretations of J_{CC} in aldopyranosyl rings regardless of their configurations and conformations and of strengthening interpretations of these couplings in potentially flexible saccharide elements such as the *O*-glycosidic linkages of oligosaccharides.

Experimental Procedures

Synthesis of ^{13}C-Labeled D-Aldoses and Methyl D-Aldopyranosides. Singly ^{13}C-labeled monosaccharides were prepared by chemical or chemo-enzymic methods. Each compound is identified in the following paragraph with the pertinent literature reference for its synthesis. Throughout this paper, [^{13}C]isotopomers are identified by a compound number and a superscript denoting the location of the labeled carbon (e.g., D-[1-^{13}C]glucose is **1**^{1}).

D-[1-^{13}C]Glucose (**1**^{1});[12] D-[2-^{13}C]glucose (**1**^{2});[12,13] D-[3-^{13}C]-glucose (**1**^{3});[12−14] D-[4-^{13}C]glucose (**1**^{4});[14] D-[5-^{13}C]glucose (**1**^{5});[14] D-[6-^{13}C]glucose (**1**^{6});[15] D-[1-^{13}C]mannose (**2**^{1});[12] D-[2-^{13}C]mannose (**2**^{2});[12,13] D-[3-^{13}C]mannose (**2**^{3});[12−14] D-[4-^{13}C]mannose (**2**^{4});[13,14] D-[5-^{13}C]mannose (**2**^{5});[13,14] D-[6-^{13}C]mannose (**2**^{6});[13,15] methyl β-D-[1-^{13}C]allopyranoside (**3**^{1});[12,16] methyl β-D-[2-^{13}C]allopyranoside (**3**^{2});[12,13,16] methyl β-D-[3-^{13}C]allopyranoside (**3**^{3});[12,13] D-[2-^{13}C]allose (**4**^{2});[12,13] D-[3-^{13}C]allose (**4**^{3});[12,13] D-[2-^{13}C]altrose (**5**^{2});[12,13] methyl α-D-[2-^{13}C]altropyranoside (**6**^{2});[12,13,16] D-[2-^{13}C]galactose (**7**^{2});[12,13] methyl α-D-[2-^{13}C]galactopyranoside (**8**^{2});[12,13,16] methyl α-D-[3-^{13}C]-galactopyranoside (**8**^{3});[12,13,16] methyl β-D-[2-^{13}C]galactopyranoside (**9**^{2});[12,13,16] methyl β-D-[3-^{13}C]galactopyranoside (**9**^{3});[12,13,16] methyl/ethyl α-D-[2-^{13}C]glucopyranoside (**10**^{2});[12,13,16] methyl α-D-[3-^{13}C]-glucopyranoside (**10**^{3});[12,13,16] methyl/ethyl β-D-[2-^{13}C]glucopyranoside (**11**^{2});[12,13,16] methyl β-D-[3-^{13}C]glucopyranoside (**11**^{3});[12,13,16] ethyl α-D-[2-^{13}C]mannopyranoside (**12**^{2});[12,13,16] ethyl β-D-[2-^{13}C]-mannopyranoside (**13**^{2});[12,13,16] D-[2-^{13}C]talose (**14**^{2});[12,13] D-[3-^{13}C]-arabinose (**15**^{3});[13,17] methyl α-D-[3-^{13}C]allopyranoside (**16**^{3});[12,13,16] and d-[3-^{13}C]xylose (**17**^{3}).[13,17]

Measurement of ^{13}C−^{13}C Spin-Coupling Constants. Solutions (∼1 mL, ∼0.1 *M*) of ^{13}C-labeled compounds in $^{2}H_2O$ (98 atom %) were prepared and transferred to 3-mm NMR tubes. 1-D ^{13}C{^{1}H} NMR spectra were obtained at 30 °C on a 600-MHz FT-NMR spectrometer operating at 150.854 MHz for ^{13}C and equipped with a 3-mm ^{13}C/^{1}H microprobe (Nalorac). Spectra were collected with a ∼10 800 Hz spectral window and ∼5 s recycle time (^{13}C T_1s were estimated to be ∼1 s under the experimental solution conditions[18]). FIDs were zero-filled once or twice to give final digital resolutions of <0.05 Hz/pt, and FIDs were processed with resolution enhancement (Gaussian or sine-bell functions) to improve resolution and facilitate the measurement of small *J*-couplings (Figure S1). The degree of enhancement was chosen empirically

(4) Bossennec, V.; Firmin, P.; Perly, B.; Berthault, P. *Magn. Reson. Chem.* **1990**, *28*, 149−155.
(5) Krivdin, L. B.; Kalabin, G. A. *Prog. NMR Spectrosc.* **1989**, *21*, 293−448.
(6) Church, T.; Carmichael, I.; Serianni, A. S. *Carbohydr. Res.* **1996**, *280*, 177−186.
(7) Bose, B.; Zhao, S.; Stenutz, R.; Cloran, F.; Bondo, P. B.; Bondo, G.; Hertz, B.; Carmichael, I.; Serianni, A. S. *J. Am. Chem. Soc.* **1998**, *120*, 11158−11173.
(8) Cloran, F.; Carmichael, I.; Serianni, A. S. *J. Am. Chem. Soc.* **1999**, *121*, 9843−9851.
(9) Serianni, A. S.; Bondo, P. B.; Zajicek, J. *J. Magn. Reson.* **1996**, *112*, 69−74.
(10) Zhao, S.; Bondo, G.; Zajicek, J.; Serianni, A. S. *Carbohydr. Res.* **1998**, *309*, 145−152.
(11) Cloran, F.; Carmichael, I.; Serianni, A. S. *J. Am. Chem. Soc.* **2000**, *122*, 396−397.
(12) Serianni, A. S.; Nunez, H. A.; Barker, R. *Carbohydr. Res.* **1979**, *72*, 71−78.
(13) Hayes, M. L.; Pennings, N. J.; Serianni, A. S.; Barker, R. *J. Am. Chem. Soc.* **1982**, *104*, 6764−6769.
(14) Serianni, A. S.; Vuorinen, T.; Bondo, P. *J. Carbohydr. Chem.* **1990**, *9*, 513−541.
(15) King-Morris, M. J.; Bondo, P. B.; Mrowca, R. A.; Serianni, A. S. *Carbohydr. Res.* **1988**, *175*, 49−58.
(16) Podlasek, C. A.; Wu, J.; Stripe, W. A.; Bondo, P. B.; Serianni, A. S. *J. Am. Chem. Soc.* **1995**, *117*, 8635−8644.
(17) Serianni, A. S.; Clark, E. L.; Barker, R. *Carbohydr. Res.* **1979**, *72*, 79−91.
(18) Serianni, A. S.; Barker, R. *J. Magn. Reson.* **1982**, *49*, 335−340.

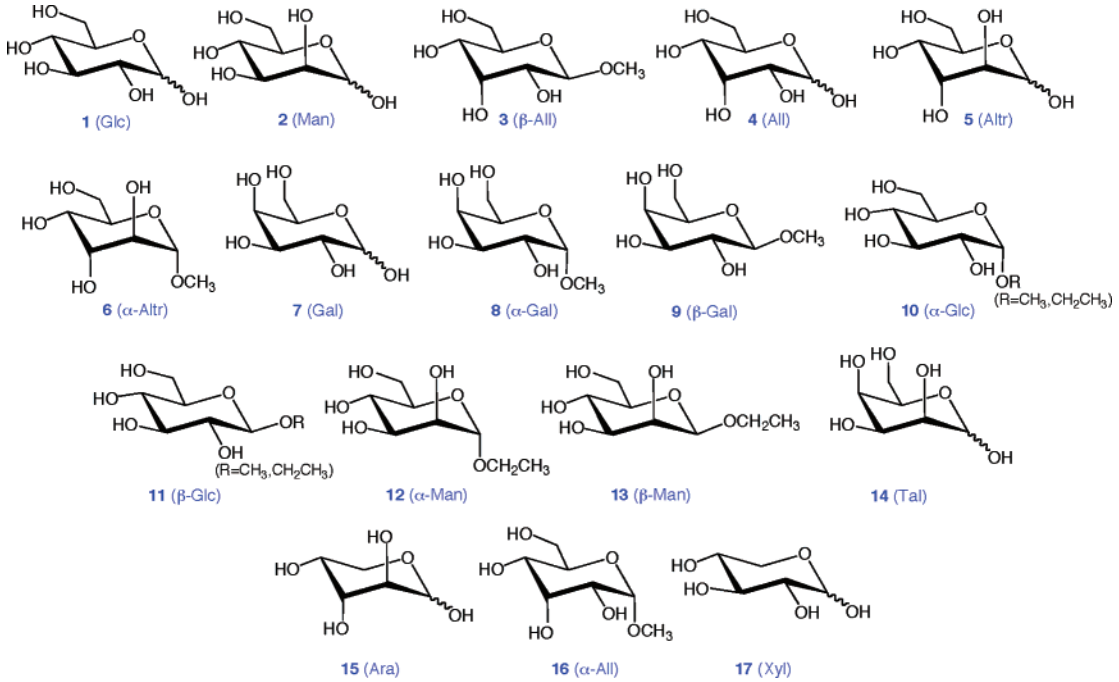

based on the spectral S/N and resolution observed in the unapodized, transformed spectrum. Line splittings greater than ~0.8 Hz were typically resolved sufficiently to permit direct measurement of the *J*-coupling with a ±0.1 Hz error, but for smaller couplings, line widths (~1 Hz) similar to, or greater than, the splitting gave larger errors (±0.2 Hz). When possible, *J*-couplings were measured in two directions (e.g., $^{1}J_{C2,C3}$ determined from [2-^{13}C]- and [3-^{13}C]-isotopomers) to quantify internal consistency, accuracy, and reproducibility. Coupling signs were assigned based on the PR rule[6] and/or on those predicted by DFT calculations.

Computational Methods

Selection and Geometric Optimization of Model Compounds. Theoretical calculations of J_{CC} were conducted on 11 methyl D-aldohexopyranosides: *β*-All (**3**^{C}), α-Alt (**6**^{C}), α-Gal (**8**^{C}), *β*-Gal (**9**^{C}), α-Glc (**10**^{C}), *β*-Glc (**11**^{C}), α-Man (**12**^{C}), *β*-Man (**13**^{C}), α-All (**16**^{C}), *β*-Alt (**18**^{C}), and *β*-Gul (**19**^{C}) (Scheme S1). The superscript C denotes structures generated *in silico* to distinguish them from those studied experimentally. DFT calculations were conducted within *Gaussian*03[19] using the B3LYP functional[20] and 6-31G* basis set[21] for geometric optimization, as described previously.[22,23] Initial geometric constraints were as follows: (a) all ring conformations were $^{4}C_1$, except for **6**^{C}, which was studied in the $^{1}C_4$ ring form; (b) exocyclic hydroxymethyl (CH_2OH) groups were set in the *gt* conformation (C4−C5−C6−O6 torsion angle of 180°) in $^{4}C_1$ structures; in **6**^{C}, the O5−C5−C6−O6 torsion angle was set at 180° (*tg* conformation); (c) C2−C1−O1−CH_3 torsion angles were set at 180° (most favored geometry based on stereoelectronic considerations[24−26]); (d) C5−C6−O6−H torsion angles were set at 180°; and (e) the remaining H2−C2−O2−H, H3−C3−O3−H, and H4−C4−O4−H torsion angles were set arbitrarily at 180° to minimize intramolecular H-bonding.

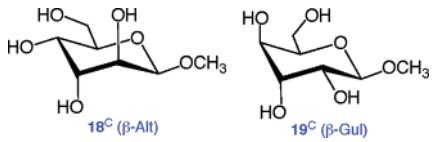

Since J_{CC} values involving internal ring carbons were a focus of attention, fully substituted model structures were chosen for study despite potential complications in the analysis of computed couplings caused by the arbitrary choice of exocyclic C−O torsions. To partially address effects caused by the latter, two sets of geometry optimizations were performed on each structure, denoted FIXED and FLOAT. In the FIXED series, all initial molecular parameters were optimized except for the exocyclic C−O torsions, which were fixed at their initial values. In the FLOAT series, all molecular parameters, including the exocyclic C−O torsions, were optimized. This approach produced the 22 optimized structures shown in Schemes S1 and S2.

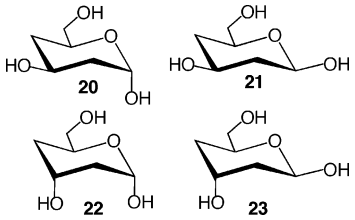

An additional series of calculations was conducted on four aldohexopyranosyl rings lacking hydroxyl groups at C2 and C4. In **20**−**23**, the four possible relative orientations of the C1−O1 and C3−O3 bonds were investigated. In each structure, the O5−C5−C6−O6 torsion angle was rotated in 30° increments through 360° and held constant, and all remaining molecular parameters were optimized. Initial C4−C3−O3−H and C5−C6−O6−H torsion angles were set at 180°.

Theoretical Calculations of $^{13}C-^{13}C$ Spin-Coupling Constants. J_{CC} values were calculated in **3**^{C}, **6**^{C}, **8**^{C}, **9**^{C}, **10**^{C}, **11**^{C}, **12**^{C},

(19) Frisch, M. J. et al. *Gaussian 03*, revision A.1; Gaussian, Inc.: Pittsburgh, PA, 2003.
(20) Becke, A. D. *J. Chem. Phys.* **1993**, *98*, 5648−5652.
(21) Hehre, W. J.; Ditchfield, R.; Pople, J. A. *J. Chem. Phys.* **1972**, *56*, 2257−2261.
(22) Cloran, F.; Zhu, Y.; Osborn, J.; Carmichael, I.; Serianni, A. S. *J. Am. Chem. Soc.* **2000**, *122*, 6435−6448.
(23) Cloran, F.; Carmichael, I.; Serianni, A. S. *J. Am. Chem. Soc.* **2001**, *123*, 4781−4791.
(24) Lemieux, R. U. *Pure Appl. Chem.* **1971**, *25*, 527−548.
(25) Praly, J.-P.; Lemieux, R. U. *Can. J. Chem.* **1987**, *65*, 213−223.
(26) Juaristi, E.; Cuevas, G. *The Anomeric Effect*; CRC Press: Boca Raton, FL, 1995.

TABLE 1. $^{13}C-^{13}C$ Spin-Couplings[a] in Selectively ^{13}C-Labeled D-Gluco- (1α, 1β) and D-Mannopyranoses (2α, 2β) and Methyl β-D-Allopyranoside 3[1]

Coupling	α-Glc*p* (**1**α)	β-Glc*p* (**1**β)	α-Man*p* (**2**α)	β-Man*p* (**2**β)	Me β-Allo*p* (**3**[1])
$^{1}J_{C1,C2}$	46.2 / 46.2[b] 46.7[e]	46.0 / 46.0 46.9	46.7 / 46.7 47.2	42.7 / 42.7 43.8	48.1
$^{2}J_{C1,C3}$	*nc* / *nc* *nc*	(+) 4.5 / (+) 4.5 (+) 4.5	*nc* / *nc* *nc*	(+) 4.0 / (+) 4.0 +3.9	*nc*
$^{2}J_{C1,C5}$	(-) 1.8 (-) 2.0	*nc* *nc*	(-) 2.0 (-) 2.0	*nc* *nc*	(±) 0.7
$^{3+3}J_{C1,C4}$	*nc* *nc*	*nc* *nc*	0.9 0.7	*nc* *nc*	*nc*
$^{3}J_{C1,C6}$	3.3 3.3	4.1 4.1	3.3 3.2	3.9 4.0	3.5
$^{1}J_{C2,C3}$	38.2 / 38.2[c] 38.2	38.8 / 38.8[c] 38.9	37.7 / 37.7[c] 37.8	38.2 / 38.8[c] 38.2	
$^{2}J_{C2,C4}$	(+) 3.1 / (+) 3.1 (+) 3.0	(+) 2.8 / (+) 2.8 (+) 2.7	*nc* / *nc* *nc*	*br* / *nc* (±) 0.3	
$^{3+3}J_{C2,C5}$	*nc* *nc*	*nc* *nc*	*br* *nc*	*nc* *nc*	
$^{1}J_{C3,C4}$	38.6 / 38.6[d] 38.5[f]	39.4 / 39.3[d] 39.3	39.9 / 39.9[d]	40.3 / 40.4[d]	
$^{2}J_{C3,C5}$	(+) 1.7 (+) 1.8	(+) 2.5 (+) 2.4	(+) 1.7	(+) 2.7	
$^{3}J_{C3,C6}$	3.8 3.7	4.3 4.2	3.7	4.2	
$^{1}J_{C4,C5}$	40.4 40.4	40.9 41.0	40.2	40.9	
$^{2}J_{C4,C6}$	*nc* *nc*	*nc* *nc*	*nc*	*nc*	
$^{1}J_{C5,C6}$	43.6 43.3	43.0 43.3	43.3	43.3	

[a] In Hz ± 0.1 Hz determined in D-glucose and D-mannose selectively ^{13}C-labeled at C1−C6; in $^{2}H_2O$ at ~25 °C. An entry of *nc* implies that $J < 0.6$ Hz; *br* denotes a broadened signal containing an unresolved coupling. Signs of $^{2}J_{CC}$ are given in parentheses. [b] Couplings in blue were reported previously (refs 2 and 3). [c] Measured in the [3-^{13}C]isotopomer. [d] Measured in the [4-^{13}C]isotopomer. [e] Couplings in brown are for the corresponding ethyl glycoside (ref 7). [f] Couplings in green are for the corresponding methyl glycoside (ref 28).

13^{C}, **16**^{C}, **18**^{C}, and **19**^{C} (Schemes S1 and S2) and in **20**−**23** with *Gaussian*03[19] using DFT (B3LYP).[20] Finite-field double perturbation theory[27a,b] was used to recover the Fermi contact, diamagnetic and paramagnetic spin−orbit, and spin−dipole terms[27c] with a [5s2p1d|3s1p] basis set,[27d] and the raw (unscaled) calculated couplings are reported. A comparison of the relative contributions of Fermi and non-Fermi contact terms to representative calculated J_{CC} values is provided in Table S1.

Results and Discussion

General Observations in 1 and 2. J_{CC} values in α- and β-gluco- (**1**α, **1**β) and manno- (**2**α, **2**β) pyranoses singly ^{13}C-labeled at C1−C6 are listed in Table 1. General trends observed in these data are summarized as follows.

$^{1}J_{CC}$ values range from 37.7−46.7 Hz, with $^{1}J_{C1,C2} > {}^{1}J_{C5,C6} > {}^{1}J_{C2,C3} \approx {}^{1}J_{C3,C4} \approx {}^{1}J_{C4,C5}$. Conversion of reducing sugars to methyl/ethyl glycosides increased $^{1}J_{C1,C2}$ by 0.5−1 Hz, with negligible effects on the remaining couplings.

$^{2}J_{C1,C5}$ values are either ~0 Hz or negative (approximately −2 Hz) and depend on anomeric configuration (more negative in α-anomers). $^{2}J_{CCC}$ values range from +4.5 Hz ($^{2}J_{C1,C3}$) to small or zero values ($^{2}J_{C4,C6}$) and are sensitive to configuration at the coupled carbon(s) (e.g., $^{2}J_{C1,C3}$ and $^{2}J_{C2,C4}$) and, in some cases, to configuration at remote carbons, the latter defined as carbons not present in the coupling pathway. For example, $^{2}J_{C3,C5}$ is ~0.8 Hz larger in the β-anomers than in the α-anomers (Table 1) even though C1 is not present in the coupling pathway.

$^{3}J_{C1,C6}$ values depend on the anomeric configuration, with couplings ~0.7 Hz smaller in α-pyranoses (~3.3 Hz) than in β-pyranoses (~4.0 Hz). $^{3}J_{C3,C6}$ values are similar in magnitude to $^{3}J_{C1,C6}$ and, like the latter, show a small dependence on anomeric configuration (α-pyranose couplings are smaller than β-pyranose couplings by ~0.5 Hz). Dual pathway couplings, $^{3+3}J_{C1,C4}$ and $^{3+3}J_{C2,C5}$, are small and are observed only in some ring configurations (e.g., $^{3+3}J_{C1,C4}$ in **2**α).

Previous studies of *gluco* and *manno* configurations provide useful insights into the dependences of J_{CC} on the saccharide structure. However, limiting investigations to two ring configurations necessarily yield incomplete data on which to develop generalized structural correlations. In addition, since not all structural factors can be studied experimentally, complementary information obtained from theoretical calculations of J_{CC} can be helpful.[22,23] In the following discussion, experimental and theoretical (DFT) analyses of J_{CC} are more completely developed and integrated in a broader range of structures, with emphasis on $^{2}J_{CC}$, $^{3}J_{CC}$, and $^{3+3}J_{CC}$.

$^{2}J_{CC}$ Coupling Constants. $^{2}J_{C1,C3}$ and $^{2}J_{C2,C4}$ values in aldopyranosyl rings are influenced largely by the orientation of electronegative substituents attached to the coupled carbons.[6,15] Ring configurations having equatorial substituents (e.g., β-D-*gluco*) give strongly positive $^{2}J_{C1,C3}$ and $^{2}J_{C2,C4}$ (approximately +2−4 Hz) (Tables 1 and 2).[6,9] Conversion of one or both terminal oxygen substituents (see **1**α, **2**α, and **3**[1] in Table 1) to axial orientations reduces the coupling, with the diaxial arrangement eliciting negative couplings[6] (e.g., $^{2}J_{C1,C3} = -2.4$ Hz in **4**α[3] and $^{2}J_{C2,C4} = -2.1$ Hz in **14**α[2]) (Tables 2 and 4).

(27) (a) Kowalewski, J.; Laaksonen, A.; Roos, B.; Siegbahn, P. *J. Chem. Phys.* **1979**, *71*, 2896−2902. (b) Helgaker, T.; Watson, M.; Handy, N. C. *J. Chem. Phys.* **2000**, *113*, 9402. (c) Sychrovsky, V.; Grafenstein, J.; Cremer, D. *J. Chem. Phys.* **2000**, 113, 3530. (d) Stenutz, R.; Carmichael, I.; Widmalm, G.; Serianni, A. S. *J. Org. Chem.* **2002**, *67*, 949−958.

(28) Thibaudeau, C.; Stenutz, R.; Hertz, B.; Klepach, T.; Zhao, S.; Wu, Q.; Carmichael, I.; Serianni, A. S. *J. Am. Chem. Soc.* **2004**, *126*, 15668−15685.

TABLE 2. $^{13}C-^{13}C$ Spin-Couplings[a] Involving C2 of Aldohexopyranoses and Alkyl Aldohexopyranosides

compound	$^1J_{C2,C1}$	$^1J_{C2,C3}$	$^2J_{C2,C4}$	$^{3+3}J_{C2,C5}$	$^3J_{C2,Me}$
β-D-Allop (**4**β^2)	47.3[b]				
Me β-D-Allop[c] (**3**^{2})	48.2	38.2	(+) 2.4	∼0	3.1
α-D-Altrop (**5**α^2)	46.1	obs[d]	∼0	1.6	
Me α-D-Altrop (**6**^{2})	47.7		∼0	1.5	3.5
β-D-Altrop (**5**β^2)	43.8 (43.9)[b]	obs	∼0	∼0	
α-D-Galp (**7**α^2)	46.0 (46.0)[b]	38.7	∼0	1.5	
Me α-D-Galp (**8**^{2})	46.4	39.5	*nc*	1.3	2.9
β-D-Galp (**7**β^2)	45.9 (45.9)[b]	39.7	∼0	∼0	
Me β-D-Galp (**9**^{2})	46.7	39.9	*nc*	*nc*	3.2
Et α-D-Glcp[e] (**10**^{2})	46.7	38.2	(+) 3.1	*nc*	2.9
Et β-D-Glcp[e] (**11**^{2})	46.9	38.9	(+) 2.7	*nc*	3.1
Et α-D-Manp[e] (**12**^{2})	47.2	37.8	*nc*	*nc*	
Et β-D-Manp[e] (**13**^{2})	43.8	38.2	(±) 0.3	*nc*	
α-D-Talop (**14**α^2)	46.4 (46.5)[b]	37.8	(−) 2.1	1.5	
β-D-Talop (**14**β^2)	42.3 (42.3)[b]	38.1	(−) 2.2	∼0	

[a] In Hz ± 0.1 Hz; in ^2H_2O at ∼25 °C. [b] Coupling reported in ref 2. [c] J_{CC} values indicate that the reported C2 and C3 chemical shifts of **3** (ref 39) are reversed. [d] Obs indicates that coupling could not be measured due to an obscured signal. [e] Couplings reported in ref 7. See definition of *nc* in Table 1.

Computed $^2J_{C1,C3}$ and $^2J_{C2,C4}$ values (Table 3) support coupling magnitude and sign predictions based on the PR method.[6] $^2J_{C1,C3}$ values in **9**^{C}, **11**^{C}, and **13**^{C} are moderately large and positive, whereas $^2J_{C1,C3}$ is negative in **16**^{C}. Comparatively, small positive (or near zero) $^2J_{C1,C3}$ values are computed in **3**^{C}, **8**^{C}, **10**^{C}, **12**^{C}, **18**^{C}, and **19**^{C}. Interestingly, $^2J_{C1,C3}$ in **6**^{C} is much larger than found experimentally, suggesting that the $^4C_1$ conformation, in which both the C1−O1 and C3−O3 bonds are axial, contributes to the experimental coupling (in the $^4C_1$ form, $^2J_{C1,C3}$ is negative, analogous to **16**^{C}; see Supporting Information). Computed $^2J_{C2,C4}$ values are moderately large and positive in **10**^{C} and **11**^{C} and are much smaller (or zero) in structures bearing an axial C−O bond at either C2 or C4.

Computed $^2J_{C1,C5}$ (Table 3) values generally confirm their dependence on anomeric configuration, with couplings of approximately −2 Hz in α-pyranoses and ∼0 Hz in β-pyranoses ($^4C_1$ forms). $^2J_{C1,C5}$ values are moderately large and negative in the $^1C_4$ form of **6**^{C} and in **19**^{C}. These data, along with the experimentally observed $^2J_{C1,C5}$ value of ±0.7 Hz in **3** (Table 1), suggest that $^2J_{C1,C5}$ may be observed in some ring structures bearing an equatorial C1−O1 bond. The large coupling predicted in **6**^{C} ($^1C_4$ form) may be partly caused by the larger C1−O5−C5 bond angle in this structure (∼117°) as compared to the other structures (114−115°); $^2J_{COC}$ values depend partly on the C−O−C bond angle, with increasing angles correlated with more negative couplings.[11]

Experimental $^2J_{C4,C6}$ values in most D-aldohexopyranosyl rings ($^4C_1$ forms) are small or zero (Table 1),[3] and an explanation is provided by the PR rule.[6] One-half of the PR component yields the same projection (0) for axial and equatorial OH groups at C4 (structures **I** and **II**, respectively) (Scheme 2). The second half of the PR component depends on hydroxymethyl group conformation, with values of 0, +1.5, and 0 correlating with *gg*, *gt*, and *tg* (structures **III**−**V**, respectively). Averaging of **I** (or **II**) with different populations of *gg*, *gt*, and *tg* will lead to a small $^2J_{C4,C6}$ value since averaged projection resultants of +0.5 to +1 correlate with small couplings (PR values of 0 yield approximately −2 Hz couplings, whereas PR values of +1.5 yield approximately +2 Hz couplings). This interpretation assumes that the PR method, which was derived using $^2J_{C1,C3}$ data primarily, can be applied to $^2J_{C4,C6}$. This uncertainty notwithstanding, the prediction is consistent with experimental observations.

The above arguments concerning $^2J_{C4,C6}$ require modification for pyranosyl rings in the $^1C_4$ conformation, and relevant projections are shown in Scheme S3 (see Supporting Information). Structures having an equatorial O4 (**VII**) should exhibit coupling behavior similar to $^4C_1$ structures, assuming similar rotameric populations about the C5−C6 bond. Indeed, $^2J_{C4,C6}$ in α-D-idopyranose is ∼0.7 Hz.[3] However, for structures bearing an axial O4 (**VI**), PR values are more positive (maximum of +3.0) than the approximately +1 observed in the $^4C_1$ forms, especially if the *gt* rotamer is highly preferred. This situation pertains to the α-D-altropyranosyl ring that exists partly in the $^1C_4$ or related twist-boat form in solution.[29] $^2J_{C4,C6}$ = 1.7 Hz in α-D-altropyranose **5**α (presumably positive in sign) and ∼0.6 Hz in β-D-altropyranose **5**β,[3] suggesting a greater percentage of $^1C_4$ conformer in aqueous solutions of the former. This conclusion is supported by $^3J_{C1,C6}$ and $^3J_{C3,C6}$ values, which are both smaller in **5**α than in **5**β.

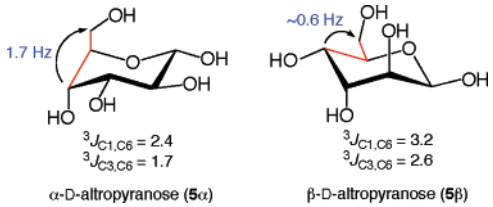

Inspection of computed $^2J_{C4,C6}$ (Table 3) reveals positive couplings ranging from 1.0−3.8 Hz. These couplings are pertinent to $^4C_1$ ring forms bearing an exocyclic CH_2OH conformation in the *gt* form in nearly all cases. Thus, correlation of a PR value of +1.5 with a $^2J_{C4,C6}$ of approximately +2 Hz is confirmed by the calculations. Variability in the computed couplings presumably reflects the slightly different C5−C6 torsion angles in the optimized structures, although other structural factors may be at work. The large positive coupling predicted in $^1C_4$ conformations is also confirmed in rings bearing an axial C4−O4 bond; the computed $^2J_{C4,C6}$ in **6**^{C} is approximately +3 Hz with a CH_2OH conformation in the *tg* state. Presumably, this coupling would be larger in the *gt* form.

The remaining $^2J_{CCC}$ in aldopyranosyl rings is $^2J_{C3,C5}$, whose properties have not been studied previously. Application of the PR method to this coupling in rings having the D-gluco configuration (Scheme S4) gives a PR value of +1.5, which translates into a predicted $^2J_{C3,C5}$ value of approximately +2 Hz. Similar treatment of the D-*galacto* configuration (O4 axial) yields the same predicted magnitude and sign (Scheme S5). However, rings having either O3 axial, or both O3 and O4 axial, yield PR values of 0, translating into $^2J_{C3,C5}$ values of approximately −2 Hz. Thus, the PR method predicts $^2J_{C3,C5}$ to be negative in the D-*allo* (O3 axial) and D-*gulo* (O3 and O4 axial) configurations. In the latter, deviation from prediction would occur if the ring assumes a conformation other than, or in addition to, $^4C_1$ (likely for α-D-*gulo*).

In **1**α/**1**β and **2**α/**2**β, $^2J_{C3,C5}$ shows a small dependence on anomeric configuration, with α-anomers giving couplings 0.8−1.0 Hz smaller than β-anomers (Table 1). Similar absolute couplings and trends are observed in **10**/**11** and **17**α/**17**β (Table 4). Conversion of O4 to an axial orientation (*galacto*)

(29) Angyal, S. J. *Angew. Chem., Int. Ed. Engl.* **1969**, *8*, 157.

TABLE 3. Computed $^2J_{CC}$ Values in Model Aldopyranosides and Comparison with Experimental Couplings

$^2J_{CC}$ (Hz)	β-All **3**^{C} FIXED	β-All **3**^{C} FLOAT	β-All **3**	α-Alt **6**^{C} FIXED	α-Alt **6**^{C} FLOAT	α-Alt **6**	α-Gal **8**^{C} FIXED	α-Gal **8**^{C} FLOAT	α-Gal **8**	β-Gal **9**^{C} FIXED	β-Gal **9**^{C} FLOAT	β-Gal **9**
$^2J_{C1,C3}$	0.9	0.9	*nc*	6.8[a]	3.6	*nc**	0.9	0.5	*nc**	7.1	6.4	+4.6*
$^2J_{C1,C5}$	-0.6	-0.5	±0.7	-1.2	-1.4	-1.6*	-2.3	-2.4	-1.9*	-0.7	-1.1	*nc**
$^2J_{C2,C4}$	1.0	0.6	+2.4	0.2	0.0	~0	0.6	-0.8	*nc*	0.3	-1.0	*nc*
$^2J_{C3,C5}$	-1.2	-1.1	-1.0	0.7	1.1		0.8	0.5	*nc*	1.1	0.9	+1.6
$^2J_{C4,C6}$	3.8	3.8	*nc**	2.5	3.6	1.7*	1.0	1.5	*nc**	1.2	1.6	*nc**

	α-Glc **10**^{C} FIXED	α-Glc **10**^{C} FLOAT	α-Glc **10**	β-Glc **11**^{C} FIXED	β-Glc **11**^{C} FLOAT	β-Glc **11**	α-Man **12**^{C} FIXED	α-Man **12**^{C} FLOAT	α-Man **12**	β-Man **13**^{C} FIXED	β-Man **13**^{C} FLOAT	β-Man **13**
$^2J_{C1,C3}$	0.6	0.7	*nc*	6.5	3.7	+4.5	-0.7	-0.3	*nc*	2.9	2.4	+3.9
$^2J_{C1,C5}$	-2.2	-2.3	-2.0	-0.5	-0.7	*nc*	-2.1	-2.2	-2.0	-0.3	-0.3	*nc*
$^2J_{C2,C4}$	3.8	3.0	+3.0	3.0	1.8	+2.7	0.4	0.1	*nc*	0.1	-0.2	±0.3
$^2J_{C3,C5}$	3.1	1.0	+1.8	3.7	1.8	+2.5*	3.3	1.0	+1.7*	4.1	1.7	+2.7*
$^2J_{C4,C6}$	2.1	1.8	*nc*	2.6	2.5	*nc*	2.1	1.7	*nc**	2.4	2.0	*nc**

	α-All **16**^{C} FIXED	α-All **16**^{C} FLOAT	α-All **16**	β-Alt **18**^{C} FIXED	β-Alt **18**^{C} FLOAT	β-Gul **19**^{C} FIXED	β-Gul **19**^{C} FLOAT
$^2J_{C1,C3}$	-1.5	-2.0	-2.4	-0.1	0.1	1.6	1.7
$^2J_{C1,C5}$	-2.1	-2.1		-0.9	-0.9	-1.1	-1.1
$^2J_{C2,C4}$	1.0	0.4		-0.6	-0.5	-0.6	-0.4
$^2J_{C3,C5}$	-0.5	-0.6	-1.1	0.1	0.1	-1.0	-1.0
$^2J_{C4,C6}$	3.0	2.9	*nc**	3.3	3.3	1.6	1.8

[a] Values in blue are couplings in FIXED and FLOAT structures (Schemes S1 and S2) that differ by >0.5 Hz. *In the corresponding reducing sugar. See definition of *nc* in Table 1.

SCHEME 2. Application of the PR Method to $^2J_{C4,C6}$ in D-Aldohexopyranosyl Rings ($^4C_1$)

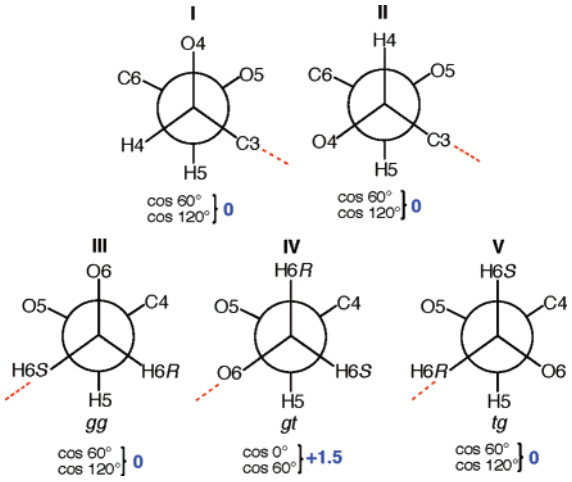

reduces $^2J_{C3,C5}$ by ~1 Hz despite PR values identical to those for *gluco* rings, but the anomeric effect is maintained (~0 Hz in **8** and +1.6 Hz in **9**) (Table 4). However, conversion of O3 to an axial orientation eliminates the effect of anomeric configuration, with **3**, **4**α, **4**β, and **16** giving virtually identical couplings (approximately −1.0 Hz) (Table 4).

Computed $^2J_{C3,C5}$ values largely confirm the predictions based on the PR method (Table 3). Couplings are positive for rings having the *gluco*, *manno*, and *galacto* configurations and negative for *allo* and *gulo* configurations. $^2J_{C3,C5}$ in **18**^{C} is unexpectedly small, suggesting that a remote effect from an axial C2−O2 bond may exist, but this was not confirmed experimentally. The computed couplings support the contention that $^2J_{C3,C5}$ depends on anomeric configuration; for α/β pairs in the *gluco* and *manno* configurations, the α-pyranose consistently gave the smaller coupling. Data for the *galacto* configuration were less conclusive.

TABLE 4. $^{13}C-^{13}C$ Spin-Couplings[a] Involving C3 of Aldohexopyranoses and Methyl Aldohexopyranosides

compound	$^1J_{C3,C2}$	$^1J_{C3,C4}$	$^2J_{C3,C1}$	$^2J_{C3,C5}$	$^3J_{C3,C6}$
α-D-Arabino*p*[b] (**15**α^3)				*nc*	
α-D-Allo*p* (**4**α^3)	37.0	37.6	(−) 2.4	(−) 1.1	2.7
Me α-D-Allo*p*[c] (**16**^{3})	37.1	37.5	(−) 2.6	(−) 1.1	2.8
β-D-Allo*p* (**4**β^3)	obs	38.6	*nc*	(−) 1.1	2.9
Me β-D-Allo*p* (**3**^{3})	38.4	38.5	*nc*	(−) 1.0	3.0
Me α-D-Gal*p*[d] (**8**^{2,3})	39.5		*nc*	*nc*	3.8
Me β-D-Gal*p*[d] (**9**^{2,3})	39.9	38.6	(+) 4.7	(+) 1.6	4.2
Me α-D-Glc*p*[d] (**10**^{3})	38.3	38.5	*nc*	(+) 1.8	3.7
Me β-D-Glc*p*[d] (**11**^{3})	39.0	39.3	(+) 4.6	(+) 2.4	4.2
α-D-Xylo*p*[b] (**17**α^3)				(+) 0.9	
β-D-Xylo*p*[b] (**17**β^3)				(+) 2.0	

[a] In Hz ± 0.1 Hz; in ^2H_2O at ~25 °C; *nc* denotes that no coupling was observed (J < 0.6 Hz). [b] Coupling reported in ref 3. [c] J_{CC} values indicate that the reported C4 and C5 chemical shifts for **16** (ref 39) are reversed. [d] Couplings reported in ref 28.

$^3J_{CC}$ Coupling Constants. $^3J_{C1,C6}$ is ~0.7 Hz larger in **1**β and **2**β than in **1**α and **2**α (Tables 1 and 5) despite similar C−O−C−C dihedral angles. Similar trends are observed[15] between **8** and **9**, and between **12** and **13**, and are reproduced in the calculations (Table 5). The terminal in-plane O1 in β-anomers enhances this coupling. A related effect also operates for $^3J_{C3,C6}$, with couplings ~0.9 Hz smaller in **3** and **16** than in **11** and **10**, respectively (Tables 4 and 5).

$^3J_{C1,C6}$ is modulated by the configuration at C3. For example, $^3J_{C1,C6}$ is 3.3 and 4.1 Hz in **1**α and **1**β (Table 1) but 2.9 and 3.3 Hz in **4**α and **4**β.[3,15] $^3J_{C1,C6}$ is also small (3.2 Hz) in β-D-altropyranose,[3,15] reinforcing the conclusion that an axial O3 truncates this coupling. While O6 orientation also affects $^3J_{C1,C6}$ (a terminal in-plane O6 found in the *tg* rotamer enhances the coupling; see Figure 1A), this factor alone cannot be

TABLE 5. Computed $^{3}J_{CC}$ and $^{3+3}J_{CC}$ Values in Model Aldopyranosides and Comparison with Experimental Couplings

$^{3}J_{CC}$ or $^{3+3}J_{CC}$ (Hz)	β-All **3**^{C} FIXED	β-All **3**^{C} FLOAT	β-All **3**	α-Alt **6**^{C} FIXED	α-Alt **6**^{C} FLOAT	α-Alt **6**	α-Gal **8**^{C} FIXED	α-Gal **8**^{C} FLOAT	α-Gal **8**	β-Gal **9**^{C} FIXED	β-Gal **9**^{C} FLOAT	β-Gal **9**
$^{3}J_{C1,C6}$	3.6	3.8	3.5	1.1	0.8	2.4*	3.9	4.0	3.6*	4.5	4.6	4.4*
$^{3}J_{C3,C6}$	3.4	3.4	3.0*	0.3	0.2	1.7*	3.9	4.4	3.7*	4.0	4.7	4.1*
$^{3+3}J_{C1,C4}$	-0.3	-0.2	*nc**	0.2	0.7	1.0*	0.0	0.3	*nc**	-0.4	-0.1	*nc**
$^{3+3}J_{C2,C5}$	0.0	0.1	~0	0.5	0.8	1.5	1.5[a]	2.1	1.3	0.2	0.6	*nc*

	α-Glc **10**^{C} FIXED	α-Glc **10**^{C} FLOAT	α-Glc **10**	β-Glc **11**^{C} FIXED	β-Glc **11**^{C} FLOAT	β-Glc **11**	α-Man **12**^{C} FIXED	α-Man **12**^{C} FLOAT	α-Man **12**	β-Man **13**^{C} FIXED	β-Man **13**^{C} FLOAT	β-Man **13**
$^{3}J_{C1,C6}$	3.7	3.9	3.3	4.4	4.4	4.1	3.7	3.7	3.2	4.4	4.4	4.0
$^{3}J_{C3,C6}$	4.3	4.8	3.7	4.6	5.1	~4.3	4.0	4.5	3.7*	4.3	4.8	4.2*
$^{3+3}J_{C1,C4}$	-0.3	-0.2	*nc*	-0.7	-0.4	*nc*	0.7	0.9	0.7	0.1	0.4	*nc*
$^{3+3}J_{C2,C5}$	0.0	0.4	*nc*	-0.5	-0.3	*nc*	0.5	1.0	*nc*	-0.1	0.0	*nc*

	α-All **16**^{C} FIXED	α-All **16**^{C} FLOAT	α-All **16**	β-Alt **18**^{C} FIXED	β-Alt **18**^{C} FLOAT	β-Alt **5**	β-Gul **19**^{C} FIXED	β-Gul **19**^{C} FLOAT
$^{3}J_{C1,C6}$	3.2	3.3	2.9*	3.6	3.8	3.2*	3.8	4.0
$^{3}J_{C3,C6}$	3.2	3.2	2.8*	3.3	3.5	2.6*	2.4	2.5
$^{3+3}J_{C1,C4}$	0.4	0.8	*nc**	1.6	1.7	1.3*	0.3	0.3
$^{3+3}J_{C2,C5}$	1.1	1.4	1.6*	0.1	0.2		1.0	1.1

[a] Values in blue are couplings in FIXED and FLOAT structures (Schemes S1 and S2) that differ by >0.5 Hz. *In the corresponding reducing sugar. See definition of *nc* in Table 1.

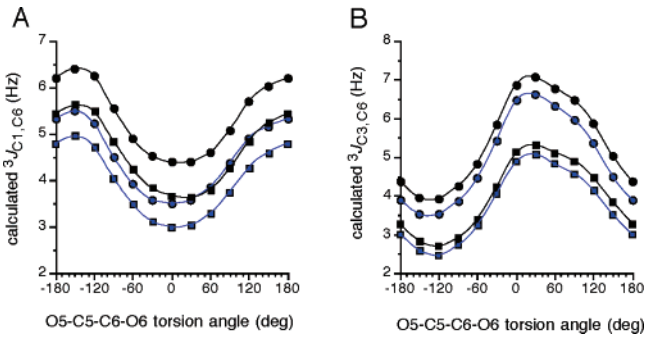

FIGURE 1. (A) Effect of exocyclic CH_2OH conformation on calculated $^{3}J_{C1,C6}$ in **20** (blue circles), **21** (black circles), **22** (blue squares), and **23** (black squares). (B) Effect of exocyclic CH_2OH conformation on calculated $^{3}J_{C3,C6}$ (same symbols as in panel A).

responsible for the observed differences since exocyclic CH_2OH conformations in the *gluco* and *allo* structures appear to be similar based on J_{HH} analysis ($^{3}J_{H5,H6}$ and $^{3}J_{H5,H6'}$ are 2.2 and 6.0 Hz, respectively, in methyl *β*-gluco- and *β*-allopyranosides[16]). Furthermore, since O6 is expected to be mostly out-of-plane in *β-gluco* structures (*gg* and *gt* rotamers are strongly favored[28]), $^{3}J_{C1,C6}$ cannot be reduced further in *β-allo* configurations by O6 effects.

Calculated $^{3}J_{C3,C6}$ values in *gluco*, *manno*, and *galacto* configurations are, in general, larger than $^{3}J_{C1,C6}$ values despite similar dihedral angles (~175°) (Table 5). However, all of the computed structures bear the exocyclic CH_2OH group in the *gt* conformation (see Computational Methods), placing the terminal O6 out-of-plane for the C1−O5−C5−C6 pathway and in-plane for the C3−C4−C5−C6 pathway. The terminal in-plane geometry contributes approximately +0.7 Hz to the coupling.[7] When this factor is taken into account, computed $^{3}J_{C1,C6}$ and $^{3}J_{C3,C6}$ become similar in magnitude. Importantly, $^{3}J_{C3,C6}$ is reduced substantially in the *allo* (**3**^{C} and **16**^{C}) and *gulo* (**19**^{C}) configurations relative to **10**^{C} and **11**^{C}, as expected since O3 is not a terminal in-plane substituent in the former. $^{3}J_{C3,C6}$ also differs in the *gulo* and *allo* configurations, with the former couplings smaller, in agreement with experimental results and with prior claims that a diaxial O3/O4 combination significantly reduces $^{3}J_{C3,C6}$ relative to the axial O3/equatorial O4 case for a C−C−C−C torsion angle of ~180°.[3]

SCHEME 3. $^{3}J_{C3,C6}$ and $^{3}J_{C1,C6}$ Coupling Pathways in 6^{C}, Showing O4 Anti to the Coupled C6 in the Former[a]

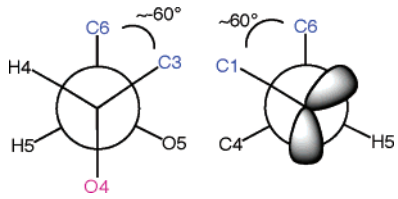

[a] Coupled carbons are in blue.

$^{3}J_{C3,C6}$ (~0.3 Hz) is smaller than $^{3}J_{C1,C6}$ (~1 Hz) in **6**^{C} despite similar torsion angles (~60°). This observation has important implications for the treatment of $^{3}J_{CC}$ values in general and is attributed to the effect of internal substituents on these couplings. Specifically, in **6**^{C}, O4 is anti to one of the coupled carbons (C6), and this arrangement reduces the gauche C−C−C−C coupling by ~1−1.5 Hz relative to that having O4 out-of-plane (i.e., when O4 is equatorial) (Scheme 3). This effect is analogous to that reported for gauche $^{3}J_{HH}$[30] and has important implications for the interpretation of dual pathway $^{3+3}J_{CC}$ values in aldopyranosyl rings, as discussed below.

Computed $^{3}J_{C1,C6}$ values in *allo* structures are uniformly smaller than corresponding values computed in the *gluco*, *manno*, and *galacto* configurations (Table 5), in agreement with the experimental findings. Thus, the remote effect of an axial O3 on the C1−O5−C5−C6 coupling pathway is captured in the DFT calculations. A similar effect is observed in **19**^{C}.

(30) (a) Günther, H. *NMR Spectroscopy*; John Wiley and Sons: New York, 1995; pp 119−120. (b) Pachler, K. G. R. *Tetrahedron* **1971**, *27*, 187−199.

SCHEME 4. Remote Effects on $^3J_{CC}$ Values in Aldohexopyranosyl Rings: Effect of C3 Configuration on $^3J_{C1,C6}$, and of C1 Configuration on $^3J_{C3,C6}$[a]

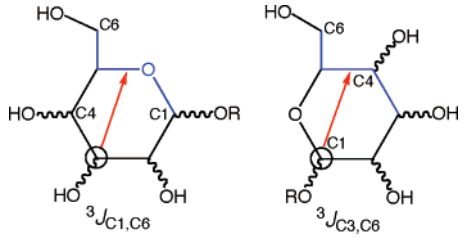

[a] Coupling pathways are in blue.

DFT calculations on **20**−**23** were conducted to validate the remote effect of O3 on $^3J_{C1,C6}$. The influence of the C5−C6 bond conformation on $^3J_{C1,C6}$ is shown in Figure 1A. The general shape of the four curves is conserved; $^3J_{C1,C6}$ is minimal at an O5−C5−C6−O6 torsion angle of 0° and is near maximal at 180°, and curve amplitudes are ∼2 Hz. This result confirms the effect of O6 orientation on $^3J_{C1,C6}$; the *tg* rotamer (O5−C5−C6−O6 torsion of 180°) produces maximal coupling since, in this conformation, O6 lies in the C1−O5−C5−C6 coupling plane. For each α/*β* pair, the α-anomer yielded smaller couplings by 0.5−1.0 Hz, confirming the effect of terminal O1 orientation on $^3J_{C1,C6}$ (the in-plane O1 found in *β*-anomers enhances the coupling). Thus, DFT calculations are consistent with experimental observations regarding the importance of terminal electronegative substituents. Importantly, the curves for **22** and **23** lie below those for **20** and **21**, respectively, despite the very similar C1−O5−C5−C6 torsion angles in these structures (−176.04 ± 1.79°), indicating that the axial O3 reduces $^3J_{C1,C6}$ in *allo* configurations regardless of the exocyclic CH_2OH conformation, again in line with experimental findings.

DFT data for $^3J_{C3,C6}$ (Figure 1B) show that this coupling is maximal at O5−C5−C6−O6 torsion angles of ∼60° (*gt* rotamer; O6 in-plane) and near minimal at approximately −120° (C4 and O6 eclipsed). The curves for **20**/**21** and **22**/**23** nearly coincide, with the latter pair displaced to smaller couplings due to the out-of-plane (axial) O3. These data also reveal a small dependence of $^3J_{C3,C6}$ on anomeric configuration, with α-anomers yielding slightly smaller couplings, in agreement with the experimental findings. The configuration at C3 influences $^3J_{C1,C6}$ values, and the configuration at C1 influences $^3J_{C3,C6}$ values; remote effects on both couplings are caused by oxygen substituents that bear the same geometric relationship to the affected coupling pathway (Scheme 4). Plots similar to those shown in Figure 1 for $^2J_{C1,C3}$, $^2J_{C1,C5}$, and $^2J_{C3,C5}$ in **20**−**23** are discussed in the Supporting Information (Figures S2−S4).

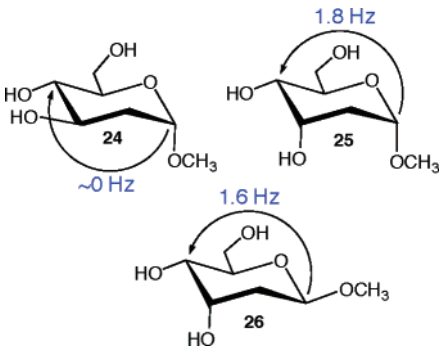

SCHEME 5. Projections about the C1′−O1′ Bond in a *β*-(1 → 4) Glycosidic Linkage Showing Two Conformations That Orient C2′ and C4 Gauche

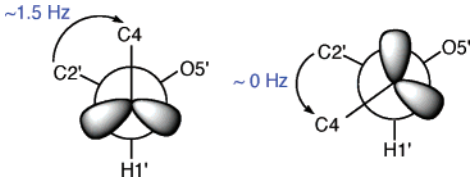

$^{3+3}J_{CC}$ Coupling Constants. Two intra-ring dual pathway $^{13}C-^{13}C$ spin−spin coupling constants exist in aldopyranosyl rings, namely, $^{3+3}J_{C1,C4}$ and $^{3+3}J_{C2,C5}$ (Scheme 1). If these couplings behave as do other dual pathway couplings,[31a] then their magnitudes and signs are determined by the algebraic sum of the couplings arising from the two constituent three-bond pathways (e.g., C1−C2−C3−C4 (front pathway) and C1−O5−C5−C4 (rear pathway) for $^{3+3}J_{C1,C4}$). The C−C−C−C and C−O−C−C torsion angles for both component pathways are approximately ±60°, and the corresponding $^3J_{CC}$ values are expected to be positive. Thus, $^{3+3}J_{CC}$ values, when observed, are expected to be positive.

$^{3+3}J_{C1,C4}$ is very small or zero in **1**α/**1***β* and **2***β* but ∼0.8 Hz in **2**α (Table 1). Experimental $^{3+3}J_{C1,C4}$ in methyl 2-deoxy-α-D-*arabino*-hexopyranoside (methyl 2-deoxy-α-D-glucopyranoside) **24** is also small, but $^{3+3}J_{C1,C4}$ in methyl 2-deoxy-α-D-*ribo*-hexopyranoside (methyl 2-deoxy-α-D-allopyranoside) **25** and methyl 2-deoxy-*β*-D-*ribo*-hexopyranoside (methyl 2-deoxy-*β*-D-allopyranoside) **26** are 1.8 and 1.6 Hz, respectively.[31b] Thus, the conversion of OH substituents from equatorial to axial orientations along the front pathway increases $^{3+3}J_{C1,C4}$ values. This observation leads to the prediction that $^{3+3}J_{C1,C4}$ should be relatively large in *β*-D-altropyranose **5***β*; indeed, a coupling of 1.3 Hz has been reported.[15]

Pertinent to providing a structural rationale for the previous observations is the fact that electronegative substituents anti to coupled hydrogens in gauche H−C−C−H coupling pathways are known to reduce $^3J_{HH}$ values.[30] A similar effect has been observed for $^3J_{CCOC}$.[32] For example, scalar couplings between C2′ and the aglycone C4 in *β*-(1 → 4) glycosidic linkages are not equivalent in the two gauche conformations, with one ∼0 Hz (O5′ anti to C4) and the other ∼1.5 Hz (H1′ anti to C4) (Scheme 5). Thus, by analogy, the C1−C2−C3−C4 coupling pathway in aldopyranosyl rings should be subject to similar effects. When O2 and O3 are equatorial, they are anti to C4 and C1, respectively, and this configuration should reduce the $^3J_{CCCC}$ along the front pathway to ∼0 Hz. When one (e.g., in **2**α) or both (e.g., in **5***β*) of these oxygens is/are axial, this reduction is mitigated, and a larger coupling is obtained. The effect appears additive, with **5***β* yielding a $^{3+3}J_{C1,C4}$ value ∼2-fold greater than observed in **2**α. Removing an equatorial substituent (deoxygenation at C2; **25** and **26**) produces a similar mitigating effect.

Configuration at the internal carbons of the front pathway appears to influence the $^{3+3}J_{C1,C4}$ values more than the orientations of the terminal electronegative substituents on the coupled carbons. This conclusion presumes that the contribution made

(31) (a) Marshall, J. L. *Carbon−Carbon and Carbon−Proton NMR Couplings: Applications to Organic Stereochemistry and Conformational Analysis*; Verlag Chemie International: Deerfield Beach, FL, 1983; pp 186−193. (b) Bose, B.; Zhang, W.; Serianni, A. S., unpublished results.

(32) Zhao, H.; Serianni, A. S., manuscript in preparation.

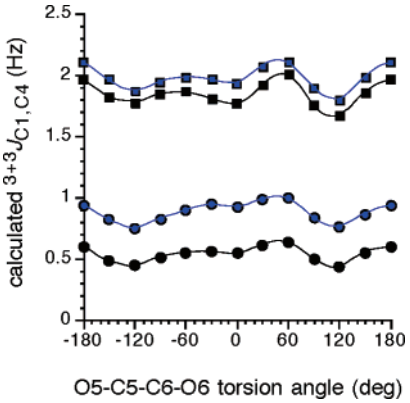

FIGURE 2. Effect of exocyclic CH_2OH conformation on calculated $^{3+3}J_{C1,C4}$ in **20** (blue circles), **21** (black circles), **22** (blue squares), and **23** (black squares).

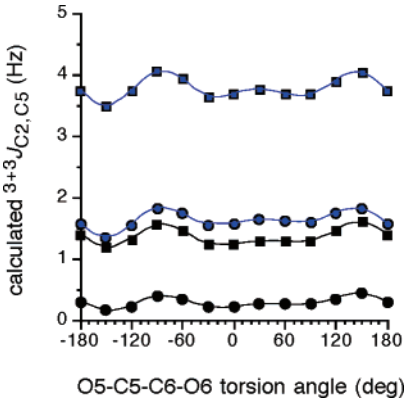

FIGURE 3. Effect of exocyclic CH_2OH conformation on calculated $^{3+3}J_{C2,C5}$ in **20** (blue circles), **21** (black circles), **22** (blue squares), and **23** (black squares).

by the rear ($^3J_{COCC}$) pathway is constant and is ∼0 Hz, that is, that this contribution is essentially unaffected by configuration at C2 and C3.

Validation of the above interpretation was obtained by calculating $^{3+3}J_{C1,C4}$ values in **20**−**23** as a function of exocyclic CH_2OH conformation (Figure 2). The calculated couplings were +0.5−1.0 Hz for **20**/**21** and approximately +2 Hz for **22**/**23**. The effect of terminal carbon configuration (anomeric configuration in this case) is much smaller than the effect of configuration at the internal C3 carbon. Structures containing an axial O3 (**22**/**23**) gave enhanced couplings by ∼1 Hz as compared to those containing an equatorial O3 (**20**/**21**). These results reaffirm the importance of internal electronegative substituent effects on $^3J_{CC}$ values for both single and dual coupling pathways.

Having developed a satisfactory structural rationale for $^{3+3}J_{C1,C4}$ behavior, the second dual pathway coupling, $^{3+3}J_{C2,C5}$, was considered. $^{3+3}J_{C2,C5}$ values are small or zero in **1**α/**1**β and **2**α/**2**β. By analogy to $^{3+3}J_{C1,C4}$, configuration at C3 and C4 should influence the C2−C3−C4−C5 pathway, and configuration at C1 should influence the C2−C1−O5−C5 pathway. In the *galacto* and *talo* configurations, $^{3+3}J_{C2,C5}$ is ∼1.5 Hz in the α-anomers and virtually zero in the corresponding β-anomers (Table 2). In these configurations, O4 is axial, and this factor presumably enhances the C2−C3−C4−C5 contribution by ∼1.5 Hz. The axial enhancement is mitigated by changing O1 from an axial to an equatorial orientation. This interpretation leads to the prediction of a nonzero coupling in β-D-gulopyranose since the two axial contributions within the C2−C3−C4−C5 pathway (O2 and O3) override the single equatorial contribution from the C2−C1−O5−C5 pathway (O1).

It is noteworthy that $^{3+3}J_{C2,C5}$ in 3-deoxy-α-D-*ribo*-hexopyranose (3-deoxy-α-D-glucopyranose) is 0.8 Hz, whereas no coupling is observed in the β-pyranose.[31b] These results further substantiate the correlation between axial oxygen substituents and $^{3+3}J_{CC}$ enhancement in aldopyranosyl rings.

The previous interpretations were tested by computing $^{3+3}J_{C2,C5}$ values in **20**−**23** as a function of exocyclic CH_2OH conformation (Figure 3). Three groups of couplings were observed: ∼0 Hz in **21**; approximately +1.5 Hz in **20** and **23**; and approximately +4 Hz in **22**. In **21**, both component pathways gave couplings of ∼0 Hz, which is consistent with both pathways containing an equatorial C−O bond (O1 and O3 are anti to C5). Each component pathway elicits a +1.5−2.0 Hz coupling in **22**, given that each contains an axial C−O bond (O1 and O3 are gauche to C5). In **20** and **23**, one component pathway contains an axial and the other an equatorial C−O bond, leading to a coupling of intermediate magnitude.

SCHEME 6

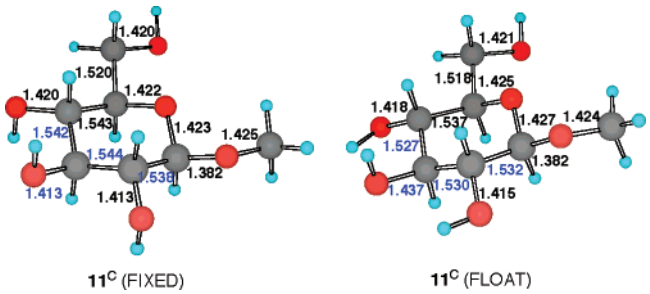

$^1J_{CC}$ Coupling Constants. With the exception of $^1J_{C1,C2}$, experimental endocyclic $^1J_{CC}$ values are typically larger in the β-anomers than in their corresponding α-anomers (Tables 1, 2, and 4). For example, $^1J_{C2,C3}$, $^1J_{C3,C4}$, and $^1J_{C4,C5}$ are 38.2, 38.6, and 40.4 Hz in **1**α and 38.8, 39.4, and 40.9 Hz in **1**β, respectively. While a structural explanation for this effect cannot be offered given the limited dataset, it may arise from slightly shorter endocyclic C−C bonds in the β-anomers resulting from different preferred exocyclic C−O bond conformations and/or other structural and stereoelectronic factors.

General Observations on Calculated J_{CC} Values. Calculated J_{CC} values in Tables 3 and 5 were determined in two conformations of each model structure that differ in the orientations of some of the hydroxyl groups. Conversion of FIXED to FLOAT structures produced changes in no (**3**^{C}, **16**^{C}, **18**^{C}, and **19**^{C}), one (**6**^{C}, **8**^{C}, **9**^{C}, **10**^{C}, **12**^{C}, and **13**^{C}), or two (**11**^{C}) C−O torsions (Schemes S1 and S2). Within each pair of structures, the FLOAT structure was consistently lower in energy by 1.3−8.5 kcal/mol. Data in Tables 3 and 5 show that exocyclic C−O torsion angles affect $^2J_{CC}$ more than $^3J_{CC}$. Specifically, exocyclic C−O torsions along a C−C−C coupling pathway ($^2J_{C1,C3}$, $^2J_{C2,C4}$, and $^2J_{C3,C5}$) influence the coupling magnitude, although the present data are too limited to decipher the underlying structural dependences. However, the data show that the rotation of specific exocyclic C−O bonds modulates saccharide structure significantly, as illustrated in a comparison of C−C and C−O bond lengths in methyl β-D-glucopyranoside **11**^{C} (FIXED) and **11**^{C} (FLOAT) (Scheme 6). The two structures contain different C1−C2−O2−H and C3−C4−O4−H torsion angles. These torsional differences induce significant bond

length changes in the vicinity of the rotated bond, with $r_{C1,C2}$, $r_{C2,C3}$, $r_{C3,O3}$, and $r_{C3,C4}$ most affected (values shown in blue). Presumably, different dispositions of the oxygen lone pairs with respect to these bonds lead to different bond lengths due to $n \rightarrow \sigma^*$ donation in some geometries. Since J_{CC} values are influenced by bond hydridization, as reflected in bond lengths, it is thus not surprising that exocyclic C−O torsions affect these couplings. Prior interpretations of $^2J_{CC}$ using the PR rule[6] have been based solely on the inspection of the relative orientation of electronegative substituents on the coupled carbons. The present results suggest that improvements in the interpretation of these geminal couplings may evolve from a more complete analysis of C−O torsional contributions at the coupled and internal carbons.

Conclusion

Correlations between aldopyranosyl ring structure and J_{CC} values have been described in this paper based on empirical analyses of experimental couplings in rings having various configurations. While some of these correlations were described in prior work, the present treatment validates and extends these correlations through theoretical *J*-coupling calculations by DFT in fully substituted aldohexopyranosyl rings, thus placing prior claims on firmer ground. In addition, new structural correlations have been proposed for $^2J_{C3,C5}$, and new insights have been obtained into the behavior of dual pathway $^{13}C-^{13}C$ couplings in aldopyranosyl rings. Remote substituent effects on J_{CC} have been identified, namely, the effects of anomeric configuration on $^2J_{C3,C5}$ and $^3J_{C3,C6}$ and the effect of C3 configuration on $^3J_{C1,C6}$. While the underlying structural and/or electronic origins of these remote effects remain unclear, documenting their existence is an important first step toward achieving this understanding, which may prove essential for more quantitative interpretations of these parameters.

The effect of anti internal oxygen substituents on gauche $^3J_{CC}$ is an important finding with long-range implications. Its existence is implicated by the internally consistent treatment of $^{3+3}J_{CC}$ values in aldopyranosyl rings described herein and, more directly, by studies of calculated $^3J_{COCC}$ across *O*-glycosidic linkages (data not shown). Studies of the arguably esoteric $^{3+3}J_{CC}$ values have thus provided, unexpectedly, new information critical to an understanding of the structurally more significant single pathway $^3J_{CC}$. While prior investigations have identified and quantified terminal electronegative substituent effects on $^3J_{CC}$, internal electronegative substituent effects have not been previously documented. The latter effects have important implications for the interpretation of trans-glycoside *J*-couplings in oligosaccharides. For example, consider the three trans-glycoside vicinal $^{13}C-^{13}C$ spin-couplings in methyl α-lactoside **27**: $^3J_{C1',C3}$, $^3J_{C1',C5}$, and $^3J_{C2',C4}$. The former two couplings are subject to terminal electronegative effects only (Scheme 7). In contrast, the latter is subject to both terminal and internal effects. The coupling pathways for the two types of $^3J_{CC}$ are therefore not equivalent, and detailed studies of this difference, which are currently underway, demonstrate that separate Karplus equations are required for quantitative treatments.

Structure−coupling correlations for $^2J_{CCC}$ and $^2J_{COC}$ are summarized in Scheme 8. Maximal $^2J_{CCC}$ (most positive) values are observed when both terminal hydroxyl substituents are equatorial, and these couplings are minimal (most negative) when both substituents are axial. Intermediate couplings are

SCHEME 7. Trans-glycoside $^3J_{COCC}$ Pathways in Methyl α-Lactoside (27) Containing Only Terminal ($^3J_{C1',C3}$; $^3J_{C1',C5}$) and Both Internal and Terminal ($^3J_{C2',C4}$) Electronegative Substituents

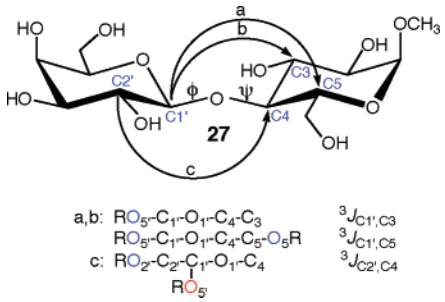

SCHEME 8. Summary of $^2J_{CC}$ Behavior in Aldopyranosyl Rings[a]

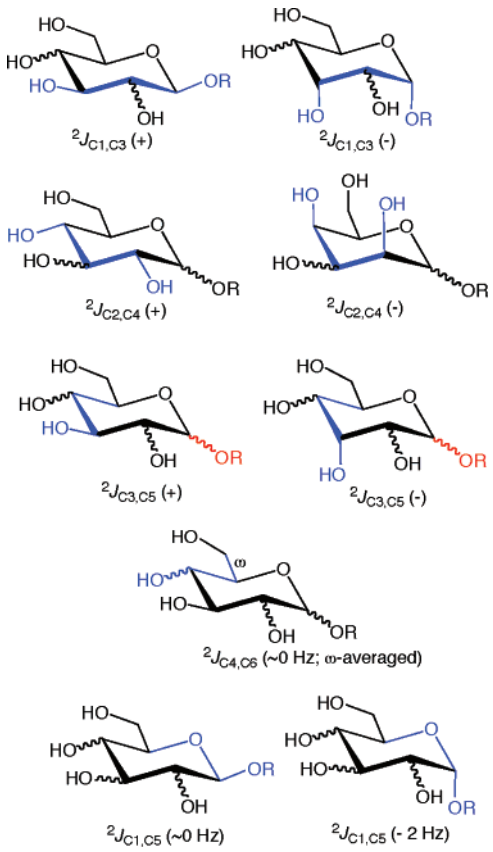

[a] Coupling pathways and direct substituent effects are in blue, and remote substituent effects are in red.

observed when one OH is axial and the other equatorial. For $^2J_{C1,C5}$, the orientation of O1 largely determines the coupling, with small or zero couplings observed when O1 is in-plane (equatorial) and negative values observed when O1 is out-of-plane (axial). For $^2J_{CCC}$, theoretical calculations reveal that C−O bond torsions involving terminal and/or intervening carbons modulate the coupling, probably in part due to the substantial bond length changes that accrue from stereoelectronic effects. This result implies that superimposed on the configurational effects at the terminal (and presumably internal) carbons are lone pair effects from the oxygens appended to the C−C−C pathway, which are modulated by C−O bond rotation. A more

SCHEME 9. Summary of $^{3}J_{CC}$ Behavior in Aldopyranosyl Rings[a]

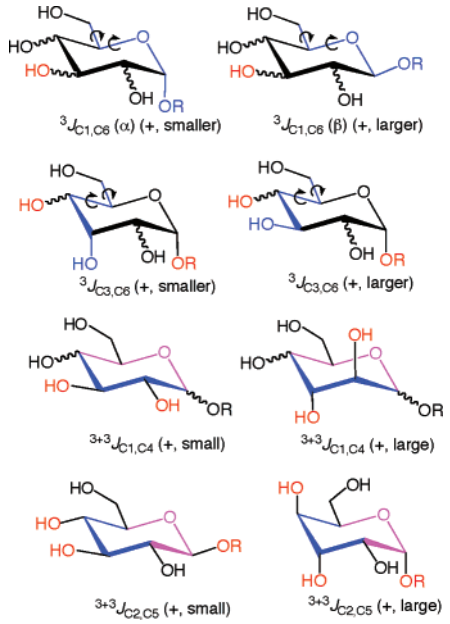

[a] Coupling pathways and direct substituent effects are in blue and pink, and remote substituent effects are in red.

systematic study of these torsional effects is presently underway, similar to that reported recently for $^{2}J_{CCH}$.[33a,b]

The remote effect of the anomeric configuration on $^{2}J_{C3,C5}$ may be due to different average conformations about the C4−O4 bond in the two anomers, possibly caused by different intra- and/or intermolecular H-bonding in solution, but this explanation will require further investigation.

Correlations involving single pathway and dual pathway $^{3}J_{CC}$ are summarized in Scheme 9. While single pathway couplings depend primarily on either a C−C−C−C or a C−C−O−C torsion angle, the electronegative atom orientation at the terminal (coupled) carbon(s) is an important secondary determinant. For $^{3}J_{C1,C6}$ and $^{3}J_{C3,C6}$, the latter factor leads to their partial dependence on exocyclic CH_2OH conformation in aldohexopyranosyl rings. $^{3}J_{C1,C6}$ and $^{3}J_{C3,C6}$ are also affected by configuration at remote carbons, with C3 configuration affecting the former and C1 configuration affecting the latter. It is noteworthy that the remote carbon bears the same structural relationship to the affected coupling pathway in both cases.[34]

New insights, substantiated by DFT calculations, have been obtained on the structural dependencies of dual pathway $^{3}J_{CC}$ in saccharides. For aldopyranosyl rings in ideal chair forms, both constituent coupling pathways orient the coupled carbons gauche. Internal OH substituents modulate $^{3+3}J_{CC}$ by either orienting gauche or anti to one or both of the terminal coupled carbons, with the former orientation contributing positively to the coupling. For $^{3+3}J_{CC}$, the axial/equatorial orientation of the terminal OH groups appears to be less important than the axial/equatorial orientation of internal OH groups. The available data support the contention that the observed coupling is determined by summing the constituent couplings directly since both are expected to be positive in sign.

The present findings add to a growing, but still incomplete, body of knowledge about the behavior of $^{13}C-^{13}C$ *J*-couplings in saccharides. The underlying motivation for this work lies partly in the expectation that, in addition to their value as structural and conformational probes, these parameters may reveal or explain important functional properties. The first step in achieving this goal is to establish correlations between structure and *J*-coupling magnitude. The second step is to draw correlations between *J*-coupling and specific functions. Since *J*-couplings provide a convenient window into electronic structure, and since electronic structure dictates reactivity, these parameters offer an opportunity to probe and understand saccharide reactivities. Recently, this connection has been established in which $^{1}J_{CH}$ values in −CHOH− groups were related to the strength of H-bonds involving the OH hydrogen.[35]

A complete repertoire of *J*-coupling/structure correlations may permit more detailed investigations of the more elusive chemical characteristics of saccharides in solution, an example being nonglycosidic C−O torsional properties. Hydroxyl groups lie on the periphery of saccharides and are thus in intimate contact with the environment. They serve as important recognition sites in saccharide−protein binding and mediate the interactions of saccharides with solvent water. That C−O torsions in saccharides in solution, or potentially in the bound state, can be evaluated indirectly through $^{1}J_{CC}$[36] or $^{1}J_{CH}$ values,[37] which are parameters not commonly associated with this type of information, is an intriguing proposition. Integrated studies of $^{1}J_{CC}$, $^{1}J_{CH}$, $^{3}J_{HCOH}$,[38] and/or $^{3}J_{CCOH}$[38] promise to provide more complete pictures of how these C−O torsions behave in solution and how they may modulate chemical and biological reactivity in the free and bound states. Apparently, innocuous changes in C−O torsions induce major changes in saccharide covalent structure that may be exploited in controlling or regulating biological function and reactivity. For example, freezing local C−O conformation(s) in the bound state could result in bond length changes that, in turn, facilitate a change in preferred global conformation and/or influence inherent chemical reactivity. The chemistry of the bound state cannot be equivalent to that of the free state if the two states display different exocyclic C−O rotamer populations. We expect further developments in this regard as future studies of the behaviors of *J*-couplings in saccharides emerge.

Acknowledgment. This work was supported by a grant (A.S.) from the National Institutes of Health (GM059239). The Notre Dame Radiation Laboratory is supported by the Office of Basic Energy Sciences of the United States Department of

(33) (a) Klepach, T.; Carmichael, I.; Serianni, A. S. *J. Am. Chem. Soc.* **2005**, *127*, 9781−9793. (b) One of the referees of this paper noted the significant difference in computed and experimental $^{2}J_{C2,C4}$ values in *β-allo* structures (Table 3). Preliminary computational results suggest that the effect of C−O bond rotation on $^{2}J_{CCC}$, which can be substantial, is primarily responsible for this difference.

(34) It is noteworthy that $^{3}J_{C1,C6}$ values in 3-deoxy-D-*ribo*-hexopyranoses (α*p*, 3.0 Hz; β*p*, 3.4 Hz) exhibit the same truncation as observed in the D-allopyranoses. An axial O3 elicits the same remote effect on the coupling as does an axial hydrogen. The effect thus correlates with the presence of an equatorial electronegative substituent at C3, which enhances the coupling, and not strictly to a change in the C3−O3 bond orientation.

(35) Maiti, N. C.; Zhu, Y.; Carmichael, I.; Serianni, A. S.; Anderson, V. E. *J. Org. Chem.* **2006**, *71*, 2878−2880.

(36) Carmichael, I.; Chipman, D. M.; Podlasek, C. A.; Serianni, A. S. *J. Am. Chem. Soc.* **1992**, *115*, 10863−10870.

(37) Serianni, A. S.; Wu, J.; Carmichael, I. *J. Am. Chem. Soc.* **1995**, *117*, 8645−8650.

(38) Zhao, H.; Pan, Q.; Zhang, W.; Carmichael, I.; Serianni, A. S. *J. Org. Chem.* **2007**, in press.

(39) Bock, K.; Pedersen, C. *Adv. Carbohydr., Chem. Biochem.* **1983**, *41*, 27.

Energy. This is Document NDRL-4703 from the Notre Dame Radiation Laboratory.

Supporting Information Available: Scheme S1: DFT structures (FIXED Series) of **3**^{C}, **6**^{C}, **8**^{C}, **9**^{C}, **10**^{C}, **11**^{C}, **12**^{C}, **13**^{C}, **16**^{C}, **18**^{C}, and **19**^{C}; Scheme S2: same DFT structures as in Scheme S1 for the FLOAT Series; Scheme S3: projections for $^{2}J_{C4,C6}$ in D-aldohexopyranosyl rings ($^{1}C_{4}$); Scheme S4: application of the PR method to $^{2}J_{C3,C5}$ in D-glucopyranosyl rings; and Scheme S5: application of PR method to $^{2}J_{C3,C5}$ in other aldohexopyranosyl rings. Figure S1: $^{13}C\{^{1}H\}$ NMR spectrum of methyl glycosides generated from Fischer glycosidation of D-[1-^{13}C]galactose, with signal assignments and J_{CC} values; Figure S2: effect of hydroxymethyl conformation on calculated $^{2}J_{C1,C3}$ in **20**−**23**; Figure S3: effect of hydroxymethyl conformation on calculated $^{2}J_{C1,C5}$ in **20**−**23**; and Figure S4: effect of hydroxymethyl conformation on calculated $^{2}J_{C3,C5}$ in **20**−**23**. Table S1: Fermi contact and non-Fermi contact contributions to computed J_{CC} in **11**^{C} and structures of **6**^{C} ($^{4}C_{1}$) FIXED and FLOAT with Cartesian coordinates; Table S2: calculated J_{CC} in **6**^{C} ($^{4}C_{1}$) (FIXED and FLOAT) and comparison of B3LYP/6-31G* and B3LYP/6-31G** *J*-coupling calculations for **11**^{C}. Complete ref 19 and Cartesian coordinates for DFT structures. This material is available free of charge via the Internet at http://pubs.acs.org.

JO0706776